Local Atomic Environment of Si Suboxides at the $SiO_2/Si(111)$ Interface Determined by Angle-Scanned Photoelectron Diffraction

S. Dreiner,[1] M. Schürmann,[1] C. Westphal,[1,2,*] and H. Zacharias[1]

[1]*Westfälische Wilhelms-Universität Münster, Physikalisches Institut, Wilhelm-Klemm-Strasse 10, 48149 Münster, Germany*
[2]*Universität Dortmund, Lehrstuhl für Experimentelle Physik 1, Otto-Hahn-Strasse 4, 44221 Dortmund, Germany*
(Received 2 January 2001)

Local environments of Si suboxides at the interface between a thermally grown SiO_2 film and Si(111) were studied by angle-scanned photoelectron diffraction. Si $2p$ core-level spectra containing chemically shifted components were recorded. The components were deconvoluted by least squares fitting and assigned to different Si oxidation states. The obtained diffraction patterns of the various suboxides exhibit different features. Comparison of these patterns with multiple scattering calculations including a multipole R-factor analysis shows that a simple chemical abrupt interface model describes well the environment of the suboxides and indicates ordered SiO_2 close to the interface.

DOI: 10.1103/PhysRevLett.86.4068 PACS numbers: 68.35.Ct, 61.14.Qp, 79.60.Dp

The thermally grown SiO_2/Si interface has been studied extensively during the last years because of the significant role of SiO_2/Si interfaces in semiconductor devices (for instance in metal-oxide-semiconductor field-effect transistors). The investigations were performed with several experimental techniques [1] including x-ray scattering [2], electron spectroscopy [3], and scanning probe microscopy [4]. It is very difficult to determine the interface structure since the interface is buried below the surface and due to the loss of long range order. Also, a large lattice mismatch between Si and silicon oxide leads to structural stress. In order to determine the structure, the experimental technique has to be sensitive to the local environment of different atoms present in various structures at the interface.

The results of previous studies can be summarized as follows: The transition from the perfect crystalline order of the Si substrate to the amorphous silicon oxide film is abrupt and occurs within one atomic layer. Within this transition region, intermediate oxidation states of Si play a central role at the boundary of silicon to silicon oxide [1]. A lot of information on the system silicon oxide on Si(111) was gained by photoemission extended fine structure (PEFS) [5] and angle resolved photoemission [6] studies. These investigations established the statistical cross-linking model [6] being in agreement with the abrupt transition at the interface. Within this model, the dangling bonds of the two sides of the interface plane are stitched together.

We report results obtained from angle resolved high-resolution core-level photoelectron spectroscopy. With sufficient energy resolution, four additional and chemically shifted components (Si^{1+}, Si^{2+}, Si^{3+}, and Si^{4+}) [3] can be resolved in a Si $2p$ photoelectron spectrum. The intensity of the photoemission current as a function of angle and/or kinetic energy depends on the local environment of the emitting atom [7]. This dependency is caused by final-state diffraction effects of the photoelectron wave. An advantage of photoelectron diffraction compared to many other surface sensitive analytic methods is the high sensitivity to the local arrangement of nearest neighbor atoms within the escape depth of the electrons. A further advantage is that no long range order is needed. Thus the method is one of only very few techniques suitable for the investigation of buried structures on an atomic scale without surface destruction. Sieger *et al.* [5] had shown in their PEFS study that the final-state diffraction effects of the chemically shifted Si $2p$ photoelectrons are well suited to investigate the local environment of the Si suboxides. We used angle-scanned photoelectron diffraction to analyze the structure of the Si suboxides in more detail.

In the past there was a controversial discussion [3,6,8,9] about the existence of the double oxidized species of Si^{2+}, and whether it is present at the interface. The photoelectron spectroscopy results by Himpsel *et al.* clearly demonstrated that the double oxidized Si species can be found within the silicon oxide film. The structure model deducted from the PEFS [5] and angle resolved photoemission [6] results proposed a local environment for Si^{2+}, which differs significantly from the other oxidation states. In this paper we present the first data showing full 2π angle-scanned photoelectron diffraction patterns of all oxidation states. Since all oxidation states show individual patterns this indicates that all species are present within the interface and that all oxidation states have their own individual local environment. We compare the experimental with simulated diffraction patterns obtained for various assumed interface structures. A subsequently performed R-factor analysis allows to determine horizontal and vertical bond lengths of silicon and silicon oxide.

Thin SiO_2 films (<10 Å) were grown by thermal oxidation. The clean (7×7)-Si(111) sample was kept at a temperature of 850 °C during exposure to pure O_2 at a pressure of 3×10^{-5} mbar for 2 min. Photoemission spectra were recorded for a photon energy of 155 eV at the U49/1-SGM beam line at BESSY II, using a hemispherical electron analyzer with an acceptance angle of $\pm 4°$. The electron energy resolution was about 50 meV and the photon energy resolution was set to 80 meV. At a fixed

 0031-9007/01/86(18)/4068(4)$15.00 © 2001 The American Physical Society

polar angle, photoemission spectra were recorded over a 180° azimuth range with an increment $\Delta\Phi = 2°$. Subsequently, a new polar angle was set with an increment of $\Delta\Theta = 2°$ and a new azimuth scan was recorded. This was repeated until the polar and azimuth range were covered ($0° < \Theta < 84°, 0° < \Phi < 180°$).

Figure 1 shows a typical photoemission spectrum of the oxidized surface after the secondary electron background has been subtracted. The photoemission spectrum of the oxidized Si(111) surface shows a line shape consisting of five components, which are the electron signal of Si^{0+} and the four oxidation states (Si^{1+}, Si^{2+}, Si^{3+}, and Si^{4+}) [3,5]. Each measured spectrum was decomposed by least squares fitting to five components, each consisting of a pair of spin-orbit split Gaussian peaks. The obtained positions and peak widths of the oxidation states agree within a few percent to previously published results [3]. Also, a peak broadening occurs with an increasing oxidation state indicating increasing local disorder for these states close to the amorphous SiO_2 film.

Figure 2 (left column) shows experimental Si $2p$ photoelectron diffraction patterns obtained for different oxidation states (Si^{1+}, Si^{2+}, Si^{3+}) recorded with $h\nu = 155$ eV photon energy. This photon energy was chosen because an electron kinetic energy of around 50 eV allows back- and forward-scattering events with nearly the same probability. Therefore information about the structure below and above the emitter is contained in the recorded diffraction patterns. The patterns display the anisotropy function $A(\Theta, \Phi) = [I(\Theta, \Phi) - I_0(\Theta)]/I_0(\Theta)$ in a strictly linear grey scale, where $I(\Theta, \Phi)$ denotes the photoelectron intensity obtained by the above-mentioned fitting procedure and $I_0(\Theta)$ denotes the mean intensity for a given polar angle. Threefold sample symmetry was used to obtain the displayed plots of 360° azimuth range. The right column of Fig. 2 displays the simulated diffraction patterns of the corresponding oxidation states. They were simulated using clusters derived from the statistical cross-linking model [6]. The calculations were performed with the MSCD package of Chen and Van Hove [10]. The electron scattering phases are derived from a partial wave expansion for a muffin-tin potential [11]. The inner potential was set to 11 eV. All simulations were carried out in the second Rehr-Albers order [12] including multiple scattering up to the fifth order. We used the multipole R factor described by Fasel *et al.* [13] to compare the results of our calculations with the experimental data.

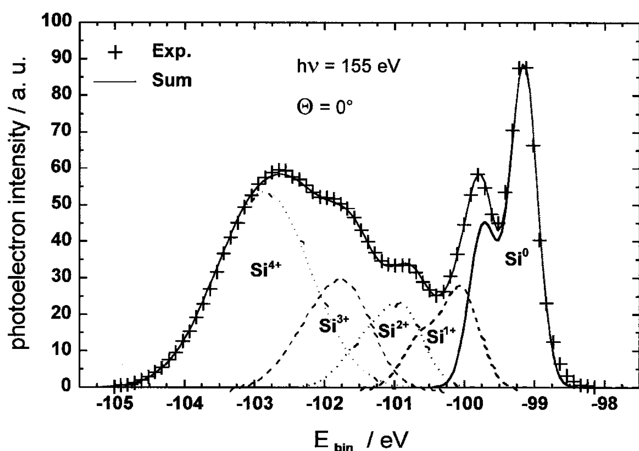

parameter:	hv= 155 eV
spin-orbit splitting	0.58 eV
Si^0 width	0.48 eV
Si^{1+} shift / width	0.9 eV / 0.59 eV
Si^{2+} shift / width	1.74 eV / 0.72 eV
Si^{3+} shift / width	2.46 eV / 0.84 eV
Si^{4+} shift / width	3.54 eV / 1.42 eV

FIG. 1. Si $2p$ core-level spectra recorded for silicon oxide on Si(111) at $\Theta = 0°$. The data points are denoted by crosses; the result of least squares fitting on this spectrum is shown as a full line. Also, the composition into Si and its four chemically shifted components due to the oxidation are shown. The table lists the peak shift and broadening of the individual components.

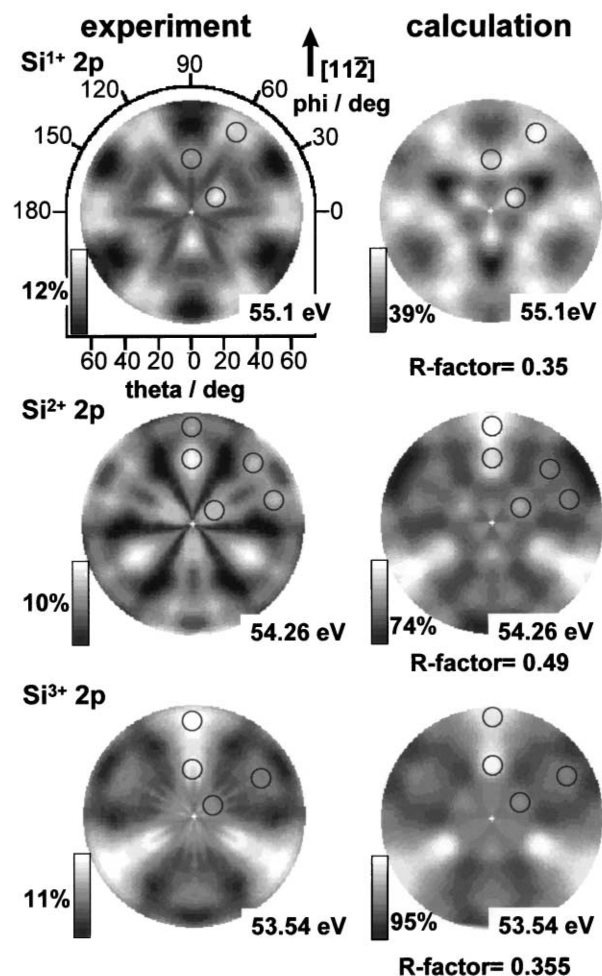

FIG. 2. Experimental (left column) and simulated (right column) Si $2p$ diffraction patterns of the silicon suboxides obtained for a photon energy of 155 eV.

The experimental diffraction patterns of the various oxidation states show intensity maxima (assigned by circles) in different directions, indicating different environments of each emitting Si^{x+}. The Si^{1+} pattern shows hexagonal arranged maxima (azimuth $\Phi = 0°, 60°, 120°, \ldots$). Also three maxima at $\Theta \approx 20°$ ($\Phi = 30°, 150°, 270°$) and the three maxima at $\Theta \approx 35°$ ($\Phi = 90°, 210°, 330°$) were found in the pattern. The Si^{2+} diffraction pattern displays maxima at $\Phi = 90°$, $\Theta \approx 40°$, and $\Theta \approx 60°$, the two maxima at $\Theta \approx 50°$ at both sides of the $\Phi = 30°$ azimuth direction, the maximum at $\Phi = 30°$ and the $\Theta \approx 20°$, and all threefold symmetry equivalent positions. For the higher oxidation state Si^{3+} an elongated maximum (consisting of two single maxima) in the $\Phi = 90°$ direction and the maximum at $\Theta = 40°$ and $\Phi = 30°$ were found. These main features are displayed in the experimental as well as in the simulated patterns. A difference between experimental and simulated diffraction patterns is the higher anisotropy obtained in the simulation. It can be explained by the perfect structure assumed in the calculation and by the effect of scattering events within the disordered SiO_2 film on the experimental diffraction patterns [14] as well as by surface roughness effects.

The experimentally observed patterns were compared with multiple scattering calculations for model clusters by an R-factor analysis. The local bonding configurations in the various oxidation states, as proposed by Luh *et al.* [6], were used as a starting point for our calculations. Their statistical cross-linking model suggests six local bonding configurations for a terminating Si atom at the interface. Each Si^{x+}-atom site is weighted by a probability function depending on the number of symmetric configurations in the cluster and on the number of bonds to oxygen atoms. Figure 3 displays the structures that were used to simulate the diffraction patterns and the parameters used in the R-factor analysis. In the simulation the structural parameters of Si-Si and Si-O bonds were varied. Parallel to the surface, the horizontal distances h_1, h_2, and h_3 were increased in steps of 5% of the silicon bulk distance (2.21 Å). For all clusters containing mainly Si-Si bonds the vertical distance v was varied by 0.05 Å steps. In the case of clusters mainly composed of Si-O bonds the vertical distance variation is replaced by a Si-O bond length variation (0.05 Å steps). The experimental and calculated diffraction patterns of the different oxidation states are discussed within the statistical cross-linking model.

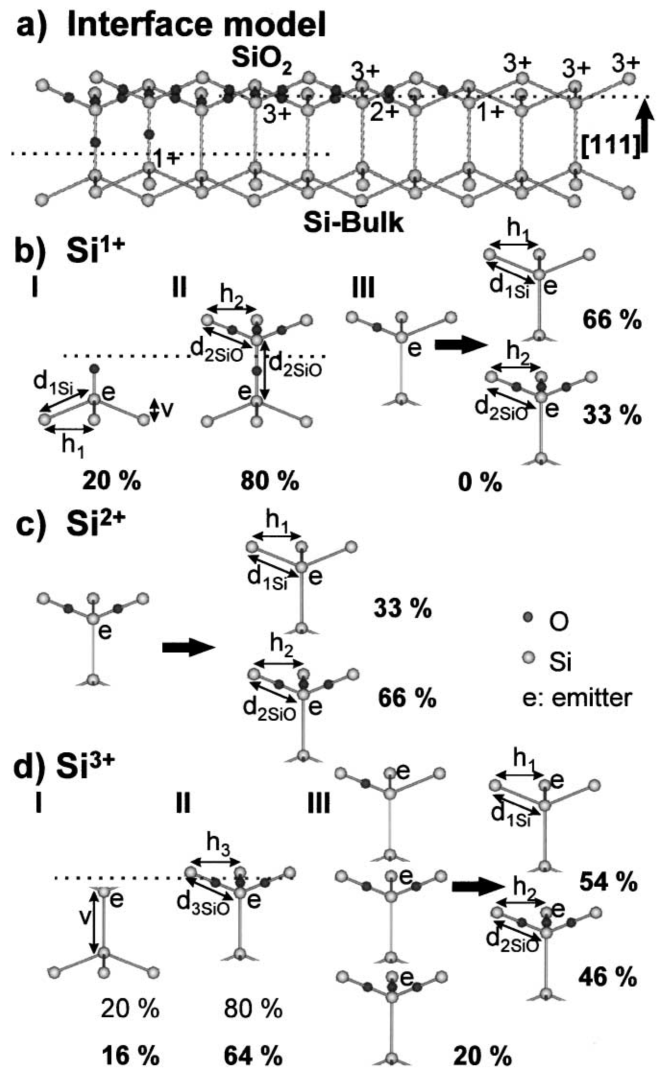

FIG. 3. Model clusters for (a) Si^{1+}, (b) Si^{2+}, and (c) Si^{3+}. In the structure the arrows indicate the parameters varied during the calculation. The parameters obtained from the R-factor analysis are (a) overview model for various suboxides found at the interface. (b) I: $h_1 = 2.32$ Å, $d_{1Si} = 2.48$ Å; II: $h_2 = 2.21$ Å, $d_{2SiO} = 3.30$ Å, III: no contribution. (c) $h_1 = 2.54$ Å, $d_{1Si} = 2.67$ Å, $h_2 = 2.21$ Å, $d_{2SiO} = 3.30$ Å. (d) I: $v = 2.35$ Å; II: $h_3 = 2.21$ Å, $d_{3SiO} = 3.30$ Å; III: $h_{1,2} = 2.21$ Å, $d_{1Si} = 2.35$ Å, $d_{2SiO} = 3.30$ Å. In structures (b) III, (c), and (d) III the displayed and all threefold symmetric clusters were included in the calculation.

Si^{1+} can be found in the upper (Figs. 3a and Fig. 3b I, II) or the lower part of a bilayer (Figs. 3a and 3b III). In Fig. 3b I a disordered SiO_2 film was assumed (not shown in the figure) and in Fig. 3b II an ordered SiO_2 layer was added to the cluster. The other possible site of Si^{1+} located in the bottom layer of a bilayer was approximated by a composition of a cluster containing only Si bonds and a cluster containing the Si-O bonds (Fig. 3b III). The results of the calculations for both clusters were superposed. The contribution of each cluster to the sum is given by the number of Si-Si bonds and the number of Si-O bonds in the original model. Below the interface, six layers of a perfect Si crystal structure were added to all used clusters. A minimal R factor of 0.35 was obtained if 80% of a diffraction pattern with and 20% without ordered SiO_2 were superposed (cf. Fig. 4). Unexpectedly, the R factor was not reduced by adding any contribution of Si^{1+} in the lower part of a bilayer. The obtained parameters for the cluster with ordered SiO_2 are $d_{2SiO} = 3.30$ Å (SiO_2 bulk distance) and $h_2 = 2.21$ Å (Si bulk value), and for clusters without ordered SiO_2 values of $d_{1Si} = 2.48$ Å and $h_1 = 2.32$ Å were obtained.

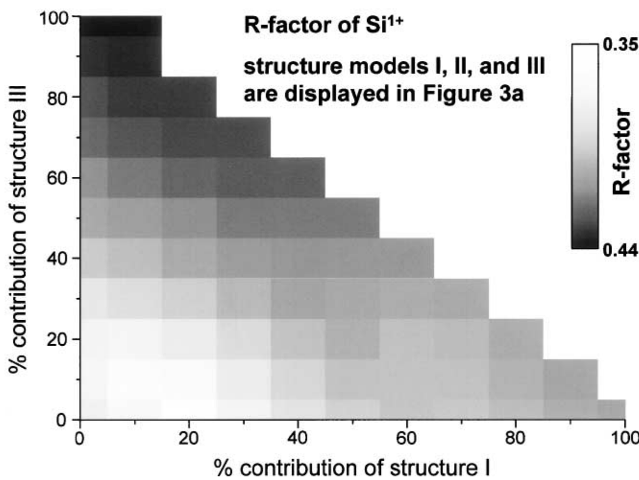

FIG. 4. R factor as a function of the composition of the interface. The absolute minimum was obtained for 20% of structure I, 0% of structure III, and 80% of structure II (structure models are displayed in Fig. 3b).

In the case of Si^{2+} we used the same approximation as in the case of Si^{1+}. The Si^{2+} can be found in a lower part of a bilayer (cf. Fig. 3c). The possible emitter environment was obtained by a superposition of the model shown in the right part of Fig. 3. The lowest R factor (0.49) was achieved for $d_{1\mathrm{Si}} = 2.67$ Å, $h_1 = 2.54$ Å, $d_{2\mathrm{SiO}} = 3.30$ Å, and $h_2 = 2.21$ Å. The R factor (0.49) is significantly higher than that obtained for Si^{1+} (0.35). This may be explained by the above-mentioned approximation. For instance, multiple scattering paths including scattering events along both Si-Si and Si-O bonds were not considered. Interestingly, within this model Si^{2+} is present only at the lower part of a bilayer. This, combined with the mean free electron path length of around 3 Å at 56 eV electron kinetic energy and combined with the low probability of Si^{2+} in the structure, leads to a weaker photoelectron signal compared to the remaining oxidation states.

The Si^{3+} situation is similar to the Si^{1+} case. We expect two different Si^{3+} sites (upper and lower layers of a bilayer). First we investigated the Si^{3+} in the bottom layer. For this, ordered SiO_2 was included (Fig. 3d II) or excluded (Fig. 3d I). The best agreement (R factor $= 0.369$) with the experiment was achieved for 80% ordered and 20% disordered SiO_2. The structural parameters were $v = 2.35$ Å (Si bulk distance) for the disordered case and $d_{2\mathrm{SiO}} = 3.40$ Å (3.30 Å SiO_2 bulk distance) and $h_2 = 2.21$ Å (Si bulk value) for the ordered case. In contrast to the Si^{1+} case the R factor was reduced from 0.369 to 0.355 if the diffraction pattern is composed of 64% of cluster I, 16% of cluster II, and 20% of cluster III (Fig. 3d). The structural parameters were $d_{2\mathrm{SiO}} = 3.3$ Å (SiO_2 bulk distance), $h_2 = 2.21$ Å, $h_1 = 2.21$ Å, and $d_{1\mathrm{SiO}} = 2.35$ Å (Si bulk values).

In conclusion we found different experimental diffraction patterns for all Si suboxides at the $SiO_2/Si(111)$ interface indicating different local environments. We compared these diffraction patterns with patterns obtained by multiple scattering calculations for clusters deduced from the simple statistical cross-linking model. The main features of the experimental diffraction patterns are well described within the simple model for the interface by the simulations. Atom positions of the suboxides within the interface were obtained from an R-factor analysis. The investigation indicates horizontally compressed silicon oxide at the interface with the bond length of SiO_2. This is obtained by the results of the R-factor analysis for all three Si suboxides, where the structure parameters of each suboxide are determined. Also, while the R-factor analysis was performed for each suboxide separately, structure parameters obtained for common atom bonds of all three suboxides (e.g., the silicon bulk distance) are in good agreement with each other. This independent confirmation supports the assumed model.

This work was supported by the Deutsche Forschungsgemeinschaft (No. We 1649/3) and by the German Federal Ministry of Education, Science, Research and Technology (BMBF) under Contract No. 05 SE8PMB 9. We thank the BESSY team for technical support during the measurements, and especially F. Senf, G. Reichardt, and W. Braun for helpful discussions.

*Corresponding author.
Email address: Carsten.Westphal@uni-muenster.de

[1] T. Hattori, Crit. Rev. Solid State Mater. Sci. **20**, 339 (1995), and references therein.
[2] I. K. Robinson, W. K. Waskiewicz, R. T. Tung, and J. Bohr, Phys. Rev. Lett. **57**, 2714 (1986).
[3] F. J. Himpsel, F. R. McFeely, A. Taleb-Ibrahimi, J. A. Yarmoff, and G. Hollinger, Phys. Rev. B **38**, 6084 (1988).
[4] F. M. Ross and J. M. Gibson, Phys. Rev. Lett. **68**, 1782 (1992).
[5] M. T. Sieger, D. A. Luh, T. Miller, and T. C. Chiang, Phys. Rev. Lett. **77**, 2758 (1996).
[6] D.-A. Luh, T. Miller, and T.-C. Chiang, Phys. Rev. Lett. **79**, 3014 (1997).
[7] C. S. Fadley, in *Synchrotron Radiation Research: Advances in Surface and Interface Science Techniques,* edited by R. Z. Bachrach, Techniques Vol. 1 (Plenum, New York, 1992), Chap. 9.
[8] T. Hattori, Appl. Surf. Sci. **130–132**, 156 (1998).
[9] D. R. Hamann, Phys. Rev. B **61**, 9899 (2000).
[10] Y. Chen and M. A. Van Hove, MSCD Package user guide, Lawrence Berkeley Laboratory (http://electron.lbl.gov/mscdpack/).
[11] F. Salvat and R. Mayol, Comput. Phys. Commun. **74**, 358 (1993).
[12] J. J Rehr and R. C. Albers, Phys. Rev. B **41**, 8139 (1990).
[13] R. Fasel, P. Aebi, J. Osterwalder, L. Schlapbach, R. G. Agostino, and G. Chiarello, Phys. Rev. B **50**, 14 516 (1994).
[14] T. Hattori, K. Hirose, H. Nohira, K. Takahashi, and T. Yagi, Appl. Surf. Sci. **144/145**, 297 (1999).